



## Formation of interleaving layers in the Bay of Bengal

Gualtiero Spiro Jaeger <sup>a,b,\*</sup>, Andrew J. Lucas <sup>c,d</sup>, Amala Mahadevan <sup>b</sup>

<sup>a</sup> Massachusetts Institute of Technology, 77 Massachusetts Ave, Cambridge, MA 02139, USA

<sup>b</sup> Woods Hole Oceanographic Institution, 266 Woods Hole Road, Woods Hole, MA 02543, USA

<sup>c</sup> Scripps Institution of Oceanography, 9500 Gilman Drive, La Jolla, CA 92093, USA

<sup>d</sup> University of California San Diego, 9500 Gilman Drive, La Jolla, CA 92093, USA



### ARTICLE INFO

#### Keywords:

Thermohaline

Stirring

Submesoscale

Eddy

Near-inertial wave

### ABSTRACT

Observations of the upper 200 m of the strongly stratified Bay of Bengal reveal a host of interleaving layers of watermass properties. The features appear as isopycnal spice anomalies and form multiple, parallel, ~10 m thin layers, that are coherent over horizontal scales of 30–80 km. They are coincident with anomalies in density stratification and in some cases, with the vertical shear of horizontal velocity, but are not aligned with isopycnals. The cross-isopycnal slopes of these prominent features are  $O(10^{-4})$  and are, on average, 5 to 10 times smaller than the expected slopes of passive tracer anomalies due to mesoscale stirring. We present two alternate mechanisms by which such interleaving layers can be created from existing lateral spice gradients: (i) stirring by vertically sheared submesoscale eddies, and (ii) near-inertial wave shear. A numerical simulation of a density (and spice) front, based on observations of a narrow and fast jet, develops a submesoscale vortex that produces spice layering similar to our observations. The layering suggests that even a weak vertical diffusivity would greatly enhance the horizontal mixing of spice at submesoscales, the scales of the proposed processes, through shear dispersion. The analysis of the observations draws attention to the prevalence of submesoscale dynamics and NIWs with unusually high vertical wavenumbers in the Bay of Bengal.

### 1. Introduction

#### 1.1. Motivation

Observations of thermohaline patterns such as intrusions, interleaving, or layering of watermasses have a history of aiding our understanding of ocean dynamics (Schmitt et al., 1987; Richards and Edwards, 2003; d'Orgeville et al., 2004). Such patterns can be generated by ocean eddies that stir watermasses together, a process that affects both dynamical and scalar property distributions and the dispersion and fluxes of important chemical and biological properties (Garrett, 1979; Toole and McDougall, 2001).

An advantage of studying thermohaline patterns alongside biogeochemical ones lies in the conserved nature of thermohaline anomalies (Flament, 2002). Since the values of the anomaly on a water parcel are set only by boundary temperature and salinity fluxes, and subsequently conserved in the ocean interior until molecularly mixed, they act as markers of the water parcels' origins and movements through the ocean interior. And unlike buoyancy or density, the density-compensated variation in temperature ( $T$ ) and salinity ( $S$ ), known as *spice*, does not directly affect the dynamics (except in the case of

double diffusion). Instead, outside of the source regions, i.e. away from boundaries, it acts as a passive tracer of the flow dynamics.

This study presents observations of thermohaline features in the Bay of Bengal (BoB) that are distinguished by the appearance of multiple, thin horizontal layers of alternating watermasses stacked one above another, in contrast to individual thermohaline intrusions characterized elsewhere (Shcherbina et al., 2009; Cole and Rudnick, 2012). Understanding the processes that create this layering is important, since it reveals the type of flow dynamics dominating horizontal stirring and watermass exchange across the basin. The characteristics of these dynamics potentially affects vertical density stratification, and thus may impact air-sea interactions in the region (Adams et al., 2019). The observed thinness of the layering created by the dynamics may also have important implications for mixing-driven fluxes, depending on the timescale of the production mechanism and the magnitude of the gradients it produces.

#### 1.2. Interleaving and the mesoscale shear and strain field

Layering in spice can be produced by mesoscale currents acting to strain and shear a large-scale horizontal gradient in watermass proper-

\* Corresponding author at: Woods Hole Oceanographic Institution, 266 Woods Hole Road, Woods Hole, MA 02543, USA.  
E-mail address: [gvsj@alum.mit.edu](mailto:gvsj@alum.mit.edu) (G.S. Jaeger).

ties (MacVean and Woods, 1980). In the typical scenario, the mesoscale horizontal shear and strain sharpens horizontal gradients in spice, while the mesoscale vertical shear differentially advects, and thus, tilts these horizontal anomalies and their horizontal gradients into long, thin, sloping layers that cross isopycnals (Haynes and Anglade, 1997). Vertical mixing acts to erase vertical spice gradients and their vertical watermass variance (Smith and Ferrari, 2009), thereby countering the production of these layers.

Just as horizontal strain cascades horizontal tracer gradients to higher wavenumbers (smaller scales), the vertical shear cascades gradients to higher vertical wavenumbers (thinner layers). This effect drives the aspect ratio, of vertical thickness to horizontal extent, towards decreasingly smaller values until it is arrested by isotropic turbulence, which erodes vertical gradients. If the ratio of mesoscale horizontal strain to mesoscale vertical shear is increased for a given vertical shear (which sets the tilt), tracer anomalies become more horizontally strained and thus thinner in the vertical. Thinner tracer features are mixed away more quickly owing to their strong vertical gradients and small vertical extents, ultimately arresting the tilting and flattening of features. Thus the ratio between horizontal strain and vertical shear determines the average slope of tracer anomalies (Smith and Ferrari, 2009). At small scales in a quasigeostrophic dynamics framework, that ratio is approximately equal to  $f/N$ , the ratio between the Coriolis parameter (inertial frequency) and vertical stratification (measured by the buoyancy frequency); (Charney, 1971).

Furthermore, while mesoscale stirring creates layers of passive tracer anomaly, such along-isopycnal currents are not expected to create coincident layers in density stratification anomaly. Yet our spatially and temporally highly-resolved observations show variability dominated by submesoscale and internal wave dynamics, which strongly influence the shear. While mesoscale stirring can create spice layering, the set of characteristics of the spice layering observed in the BoB raises the question of what alternative mechanisms could create such features.

To assess this, we present two simple conceptual mechanisms by which these processes can create thermohaline patterns observed in the uniquely detailed observations of horizontal and vertical variability of watermass properties in the BoB. We use numerical modeling to illustrate heuristically how these dynamics act to generate the observed patterns. And finally, we indicate some potential impacts on the regional oceanography, particularly in terms of expected mixing.

## 2. Methods

### 2.1. Region of study

The Bay of Bengal (Fig. 1) in the northern Indian Ocean is subject to intense monsoonal rains and immense riverine runoff, making it the freshest ocean basin in the world. Its density in the upper ~50 m is governed by salinity (Jaeger and Mahadevan, 2018) and is significantly lower than that of the underlying waters, creating an exceptionally strong density stratification beneath the surface mixed layer (Shroyer et al., 2019). This strong density stratification inhibits turbulence and thus ventilation of the thermocline. The BoB waters are in strong contrast to Arabian Sea and equatorial Indian ocean waters also found in the Bay, which are much saltier on any given isopycnal and thus offer contrasting spice characteristics to act as tracers of the local thermocline dynamics.

### 2.2. Observations

Hydrographic profiling measurements of the upper ocean were made in the Bay of Bengal between August 24th and September 20th, 2015, aboard the *R/V Revelle*, as part of the Office of Naval Research Air Sea Interaction Research Initiative (ASIRI; Fig. 1). The hydrographic

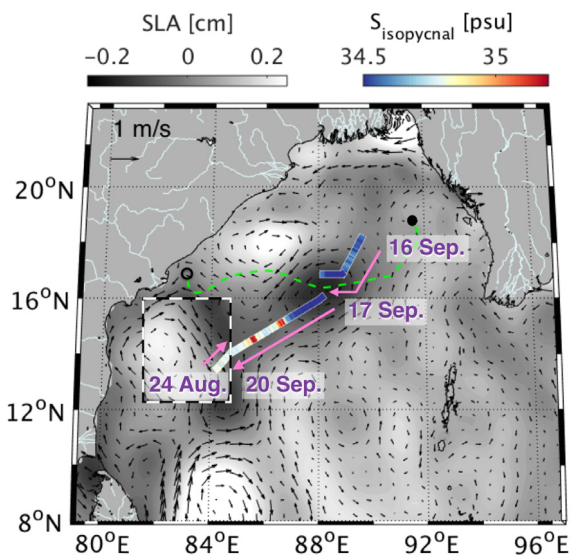


**Fig. 1.** Map of the sea level anomaly (gray shades) and associated geostrophic surface currents (arrows) in the Bay of Bengal on September 17, 2015 (inset: August 24), approximately coincident with the ship transects, along which we show salinity at the  $23\sigma$  isopycnal surface (blue to red color, pink arrows indicate ship direction). The ship sections through the large cyclonic eddy (negative SLA) revealed anomalously fresh-cold water (marked blue) in the upper 100 m of its core, compared to water outside the eddy. The dashed green line shows the track of the center of this eddy over 10 months. It formed around April 1, 2015 in the east (filled black circle), traveled westward, and merged into the East India Coastal Current around February 1, 2016 (open black circle). (For interpretation of the references to colour in this figure legend, the reader is referred to the web version of this article.)

survey was conducted with a Seabird Electronics conductivity, temperature, and pressure probe (SBE 49 CTD) mounted in a rapid profiling body and winched at high vertical speeds (approaching 10 knots) while telemetering real-time data. This system, known as the 'Fast'-CTD (FCTD) (Pinkel et al., 2012), produced vertical temperature, salinity, and pressure profiles of the upper 200 m of the ocean every ~3 min while the ship was underway at about 4 kn, mapping water property distributions on sections exceeding 1000 km, with individual profiles spaced ~300 m in the horizontal (Fig. 1). The profiler sampled at 16 Hz, which at free-fall speeds of  $4\text{--}5 \text{ m s}^{-1}$  recorded between 3 to 4 samples per meter in the vertical, resolving vertical gradients at scales of 1 m. The raw conductivity and temperature profiles were quality-controlled, and combined with a small temporal offset to maximize high-frequency lag-correlation (the variable lag, on average about one data point in length, reduced salinity spiking and associated stratification variance). Temperature and salinity were then smoothed with a 5-point median filter, and vertically binned on a regular depth grid. Further details on the FCTD instrumentation and data processing methods are described in Jaeger et al. (submitted to JPO). The anomalies discussed in this paper are well-resolved by the FCTD profiling; they are greater in magnitude ( $\gtrsim 0.1 \text{ kg m}^{-3}$ ) and occur over a larger vertical extent ( $\gtrsim 10 \text{ m}$ ) than the noise associated with salinity spiking, and are coherent over dozens or hundreds of profiles.

Ocean velocities within the upper 200 m of the ocean were measured by several (hull-, well-, and side-mounted) sonar transducers. This study uses velocities and velocity gradients (shear) measured by a 140 kHz Hydrographic Doppler Sonar System (HDSS) (Pinkel et al., 2003) that is permanently mounted on the *R/V Revelle* and configured to sample and bin data in 3 m vertical bins from 20 m to ~200 m depth. Additionally, a 300 kHz RD Instruments acoustic Doppler current profiler, temporarily installed at the bottom of a vertical pole attached to the side of the ship's hull, sampled from 10 to 50 m depth with 1 m vertical bins. The raw velocities perpendicular and parallel to

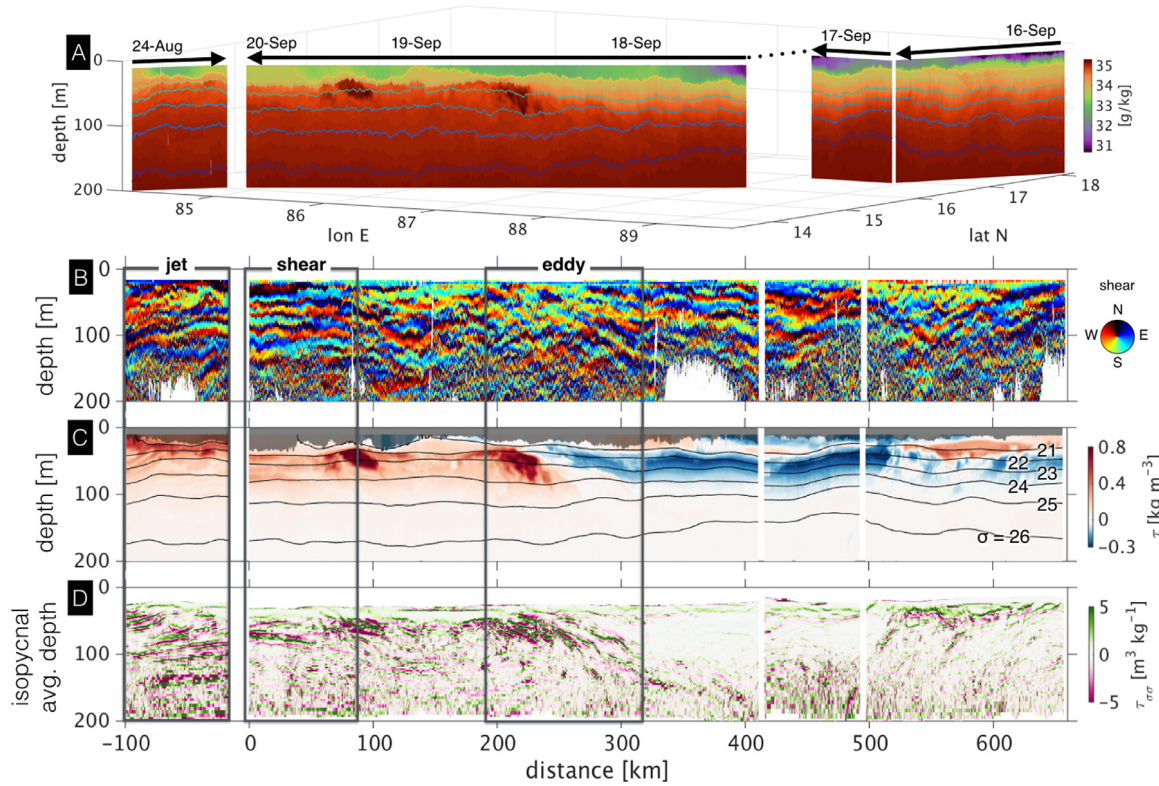


**Fig. 2.** Lateral view of the sections mapped in Fig. 1. (A) Salinity in the upper 200 m, plotted vs. latitude and longitude. The arrows and dates at the top of the sections mark the ship's passage. Thin lines mark isopycnals 21 to 26  $\sigma$ . (B) Cardinal direction of the vertical shear measured by the R/V Revelle's 140 kHz HDSS with 3 m vertical bins in the upper 200 m. The rotary shear is due to NIWs. The 4 sections, horizontally mapped to along-section distance, are shown next to each other; note though that the relative position has been adjusted for clarity of presentation. Boxes mark the regions shown in detail in Fig. 5. (C) Spice ( $\tau$ ), defined as the along-isopycnal watermass anomaly from a reference (defined as a smoothed average)  $TS$  profile. The individual spice profiles along the section have been vertically mapped to isopycnal depth, locally averaged over  $\sim 10$  km, to remove the high-frequency vertical heave and strain, but retain the average sloping features of the isopycnals. Black lines mark isopycnals, gray shading marks the surface mixed layer depth, defined by a 0.1  $\sigma$  increase in density from the surface. (D) Diapycnal Spiciness Curvature (DSC or  $\tau_{\sigma\sigma}$ ), vertically mapped to isopycnal depth averaged within each section (thus, isopycnals are flat).

the ship's direction, and their vertical gradients (shears), were quality controlled, processed into 1 min averages and rotated to eastward and northward velocity components, as well as across-track  $U$  and along-track  $V$  components. The independent measurements from the different sonar systems matched well in the overlapping depth ranges.

### 2.3. Analysis techniques

For the following analysis, temperature ( $T$ ), salinity ( $S$ ), and pressure ( $P$ ) profiles were vertically interpolated onto a density grid to calculate along-isopycnal averages and anomalies from the isopycnal average. In order to graphically present distance-depth sections without the visual contamination of highly variable vertical displacements of neighboring profiles caused by internal waves, the density-interpolated profiles are mapped to a vertical coordinate equal to the depth of the section-mean density. This removes the effect of isopycnal heaving, while preserving the average vertical isopycnal spacing and presenting isopycnals as flat horizontal lines (Fig. 2).

Since vertical profiles of horizontal current velocity were measured from ship-board transducers, and not in-situ by a lowered instrument with coincident  $TS$  measurements, horizontal velocity cannot be directly interpolated onto the same isopycnal grid as  $T$  and  $S$ .  $TS$  profiles measured by the FCTD profiler are horizontally more widely spaced, but vertically more finely resolved, than the HDSS velocity and shear profiles. They are horizontally and vertically interpolated onto the velocity profiles. Even though the interpolation imperfectly matches density to velocity bins, and vertical heave affects the current profiles (Fig. 2B), the isopycnally adjusted current and shear can be compared with the isopycnal  $TS$  and derived quantities.

Thermohaline watermass contrasts are revealed by calculating isopycnal spice (Fig. 2C). Spice is defined along an isopycnal as  $\tau = \alpha dT + \beta dS$ , where  $dT$  and  $dS$  are the difference in  $T$  and  $S$  from the reference  $T(\sigma)$ ,  $S(\sigma)$  values at potential density  $\sigma$ , and  $\alpha$  and  $\beta$  are the thermal expansion and haline contraction coefficients at  $T(\sigma)$ ,  $S(\sigma)$ , respectively (Flament, 2002). The reference  $T(\sigma)$ ,  $S(\sigma)$  profiles are created from the density-gridded sections of  $T$  and  $S$ , by finding the median  $T$  and  $S$  values for each value of  $\sigma$ , and then smoothing the profile.

Vertical changes in watermass are identified by diapycnal spiciness curvature (DSC) defined by Shcherbina et al. (2009) as

$$\tau_{\sigma\sigma} = \frac{1}{\sigma_z} \frac{d}{dz} \left( \frac{\alpha T_z + \beta S_z}{-\alpha T_z + \beta S_z} \right) \approx 2\alpha\rho T_{zz} \approx 2\beta\rho S_{zz}. \quad (1)$$

Under typical ocean conditions, where  $\alpha_z T_z \ll \alpha T_{zz}$  and  $\beta_z S_z \ll \beta S_{zz}$ , DSC can be well approximated as  $2\alpha\rho T_{zz}$  or  $2\beta\rho S_{zz}$ . DSC anomalies mark peaks in curvature in  $TS$  space, effectively highlighting the local maxima and minima in isopycnal spice along a vertical profile (Fig. 2D). DSC is equivalent to, and conveniently calculated as the vertical gradient in density space of the tangent of the Turner angle,  $Tu$ , i.e.  $\tau_{\sigma\sigma} = \frac{d}{d\sigma}(\tan Tu)$  (Shcherbina et al., 2009). The Turner angle  $Tu \equiv \tan^{-1}(\alpha T_z + \beta S_z)/(\alpha T_z - \beta S_z)$  can be computed by numerical seawater processing and analysis tool-kits. Besides being easily computed, DSC has several other benefits. Unlike spice, DSC is independent of any definition of a reference  $TS$  profile. It is also independent of vertical strain or density stratification, and is sensitive only to thermohaline watermass layering. It is a useful metric to identify vertical changes in watermass characteristics.

The ratio of vertical to horizontal gradients in DSC provides a measure of the slope of the features in watermass anomaly. Here, since we

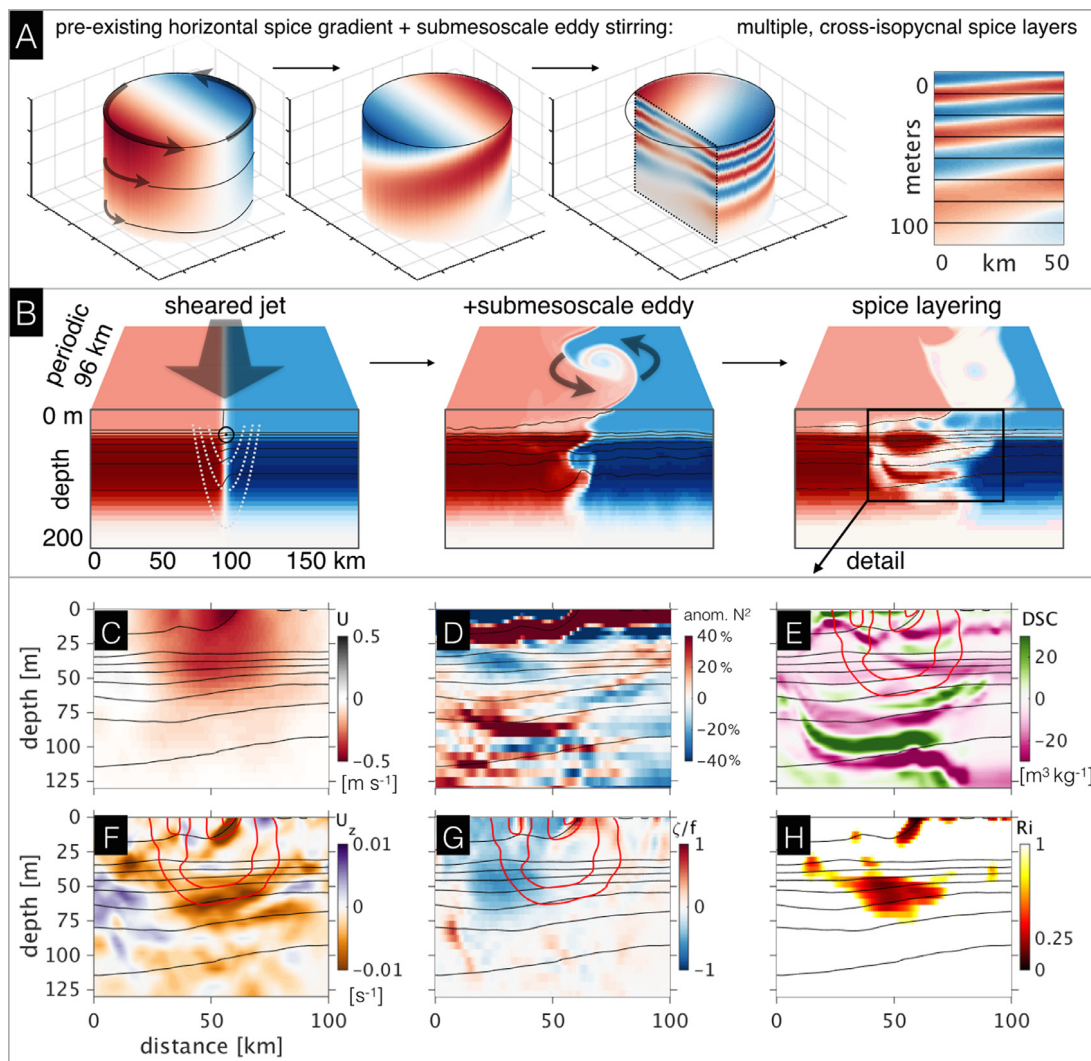


**Fig. 3.** Model simulation that shows how a submesoscale eddy along a watermass and density front can create spice interleaving. (A) Kinematic model shows a sequence of the process: An along-isopycnal gradient of spice (red to blue) is advected by along-isopycnal currents that are vertically decaying with depth. The sheared currents tilt the spice front, and after multiple rotations, multiple coherent layers of alternating watermass are formed across isopycnals. The slope of the layers decreases with time and eddy rotations, and depends on the depth and location of the transect relative to the eddy center. (B) Idealized numerical model simulation of a density front that forms submesoscale eddies that create interleaving. (Left) The initial set-up of a density (and spice) front in a ~200 km wide channel leads to a along-front jet with velocity shear in the vertical, which develops instabilities that grow into a submesoscale eddy (middle). The combination of across-front circulation and vertical shear produces interleaving layers of spice (right). Three snapshots shown are at  $t = 0$ ,  $t = 11$ , and  $t = 47$  days. Black rectangle marks the position of the following detail sections. (C) Along-channel (across-section) velocity. Red color marks out-of-page flow, black lines mark isopycnals in  $1 \text{ kg m}^{-3}$  increments, also shown in the following panels. (D) Anomaly of density stratification  $N^2$  (%) relative to depth-mean value. (E) Diapycnal Spiciness Curvature. Note the coincidence of DSC and  $N^2$  anomaly layers. Red contours mark current magnitudes (out of the page) in  $10 \text{ cm s}^{-1}$  increments, also shown in the following panels. (F) Vertical shear, across-section component, (G) Rossby number, calculated as vorticity normalized by the Coriolis parameter, (H) Richardson number, defined as  $N^2/\text{Shear}^2$ . Smaller values around 0.25 are indicative of enhanced shear production of turbulence. (For interpretation of the references to colour in this figure legend, the reader is referred to the web version of this article.)

are interested in measuring the slope distribution of the patterns of long spice layers coherent over tens of kilometers, we reduced the short-scale noise by applying a short-scale two-dimensional smoothing filter to the DSC sections before computing the slopes. The slope distribution is not very sensitive to the scale or strength of the smoothing, as long as some smoothing is applied to remove variance at the shortest resolved scale. The validity of the slope distribution is confirmed by measuring the actual slopes of the prominent layers, which is close to, and still somewhat smaller than the slope of the center of the distribution.

#### 2.4. Models

Two classes of models are used to illustrate and test hypothesized mechanisms of spice layering. First, a simple kinematic model was created to visualize the effects of different motions advecting a tracer in a column of water. A tracer field containing a horizontal gradient

was defined on a 3-dimensional grid, as seen in the first panels of Fig. 3A and Fig. 4A. To simulate an eddy (Fig. 3A), horizontal rigid-body rotation is prescribed at each vertical level of the grid, with its velocity decreasing with depth such that the vertical shear magnitude is constant. To simulate the oscillation of a near-inertial wave (NIW) (Fig. 4A), each vertical level is moved horizontally by a horizontal velocity vector of constant magnitude that is circularly rotating in direction with increasing depth. Thus the initial direction of motion of each level is depth dependent, such that there is a rotating shear similar to a downward-propagating NIW. The full column contains several vertical wavelengths. On applying these flow fields over a specified time interval to the initial tracer grid, the final position of each initial grid cell can be easily calculated. The tracer values at these new scattered positions can then be interpolated back onto the original grid, and the advected tracer patterns visualized by plotting sections.

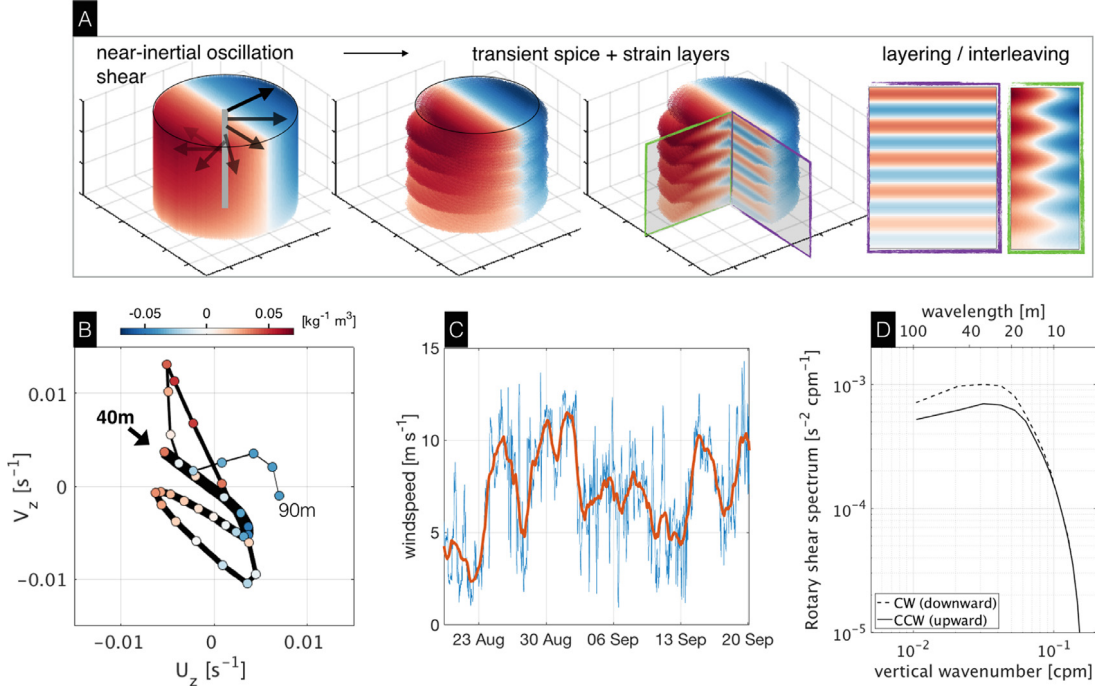


**Fig. 4.** Kinematic model of a vertically sheared near-inertial wave oscillation acting on a watermass gradient creating spice interleaving. (A) Mechanistic sequence of the proposed NIW spice interleaving process: An along-isopycnal gradient of spice (red to blue) is advected by along-isopycnal motions in different directions depending on depth. Depending on the transect orientation relative to the spice front orientation, either interleaving wiggles or horizontal layers of spice are observed. The vertical wavelength of the wave sets the vertical wavelength of the spice layering. (B) Hodograph of a vertical shear profile through the 'shear' section (location marked by black arrow in Fig. 5), colored by spice ( $\tau$ ). Thickness of the black line indicates the depth along the profile, going from 40 m (thick) to 90 m (thin). (C) Wind speed encountered during the 2015 cruise may have contributed to the generation of a strong NIW field. Blue line shows the hourly mean, orange line the 24 h mean wind speed. The prevailing direction was southwesterly, though individual squalls and rainstorms blew from other directions too. The 'shear' section was made at the very end of the cruise. (D) A spectral decomposition of shear in vertical wavenumber space, measured by a shipboard 140 kHz HDSS acoustic Doppler sonar system during the 2015 cruise reveals an excess of clock-wise rotating components, indicative of downward propagating near-inertial oscillations. (For interpretation of the references to colour in this figure legend, the reader is referred to the web version of this article.)

Secondly, we use a three-dimensional Process Study Ocean Model (PSOM) (Mahadevan et al., 1996), a finite volume fluid dynamical numerical model, at 1 km horizontal resolution, to simulate the submesoscale flow field (Mahadevan, 2006). The model is run in a periodic channel, with an across-channel width of 192 km between solid boundaries, and an along-channel length of 96 km (Fig. 3B) between periodic boundaries. The vertical grid of the model contained 64-levels, with the average vertical cell thickness increasing with depth and varying from about 3 m thickness near the surface to 5 m thickness at 100 m depth, and coarser vertical resolution extending to a maximum depth of 500 m. The model is meant to demonstrate the processes that we hypothesize as leading to watermass interleaving.

Initial conditions in the periodic channel describe a sharp density front with a coincident spice gradient. The initial density front is created by horizontally interpolating between two *TS* depth-profiles with a *tanh* function. The two profiles have the same *TS* values at depths below 100 m, but have a difference in density and scalar watermass properties above 100 m that increases towards the surface. Beneath the 30 m deep mixed layer, the interpolation between the two profiles produces a pycnocline with sharply tilted isopycnals (Fig. 3B). To initiate the development of submesoscale instabilities, the sharpness of the front is somewhat exaggerated, so that Ertel potential vorticity is negative at the front. This density front is initially balanced by a geostrophic along-front current, narrowly focused in a jet that decays with depth.

### 3. Results

#### 3.1. Hydrography and mesoscale setting

During the late monsoon period of 2015, the waters of the upper 200 m of the central Bay of Bengal were characterized by a relatively

fresh ( $31\text{--}33 \text{ g kg}^{-1}$ ) and warm ( $\sim 30^\circ \text{ C}$ ) surface mixed layer (ML) between 10 m and 30 m deep, beneath which a sharp halocline (salinity increasing to  $35 \text{ g kg}^{-1}$ ) and more gradual thermocline form a strongly stratified upper ocean. Density ranged from  $1019 \text{ kg m}^{-3}$  ( $\sigma = 19$ ) in the freshest surface layers, to  $1026.5 \text{ kg m}^{-3}$  ( $\sigma = 26.5$ ) around 200 m depth. Beneath the ML, density stratification, expressed in terms of the vertical buoyancy gradient  $N^2 \equiv -\frac{g}{\rho_0} \frac{\partial \rho}{\partial z}$ , was strong in the upper 50 m (peak  $N^2 \sim 1.5 \times 10^{-3} \text{ s}^{-2}$ ), and weakened with depth ( $N^2 \sim 1 \times 10^{-4} \text{ s}^{-2}$  at 200 m). Equivalently, buoyancy frequencies  $N$  ( $\equiv \sqrt{N^2}$ ) ranged from about  $0.04 \text{ s}^{-1}$  to  $0.01 \text{ s}^{-1}$ , equivalent to oscillation periods ( $\equiv 2\pi/N$ ) of about 2 to 10 min. The average vertical gradients of both temperature and salinity were individually stable, with only occasional small-scale inversions, such as beneath two  $\sim 50$  km long patches of salinity maxima at 50 m depth that were measured in the long ship section. Vertical shear was dominated by high-wavenumber shear layers, with an average root mean square magnitude of  $0.01 \text{ s}^{-1}$  in the upper 200 m (vector direction of vertical shear shown in Fig. 2B, see also Adams et al. (2019)).

The observing ship encountered two major mesoscale features visible in sea level anomaly (SLA) maps in Fig. 1. At the beginning of the cruise (around August 24), the ship crossed a strong frontal jet directed southeastward and offshore between a positive and negative SLA. The map inset in Fig. 1 shows the flow field around August 24 in this region, which lies approximately between  $12^\circ\text{--}16^\circ \text{N}$  and  $82^\circ\text{--}85^\circ \text{E}$ . The jet was crossed three times as the ship traversed NE, SW and then NE, with circa 100 km long repeat sections. Towards the end of the cruise and on the return leg, from September 16–20, the ship transected a  $\sim 300$  km wide cyclonic eddy with a  $\sim 17$  cm depression in SLA centered at  $88^\circ\text{E}, 16^\circ\text{N}$ . Profiling measurements from the ship made up 3 sections that cumulatively spanned about 650 km (Fig. 2).

The mesoscale eddy, which dominated surface currents and SLA, also had an imprint in the hydrography below the surface mixed layer.

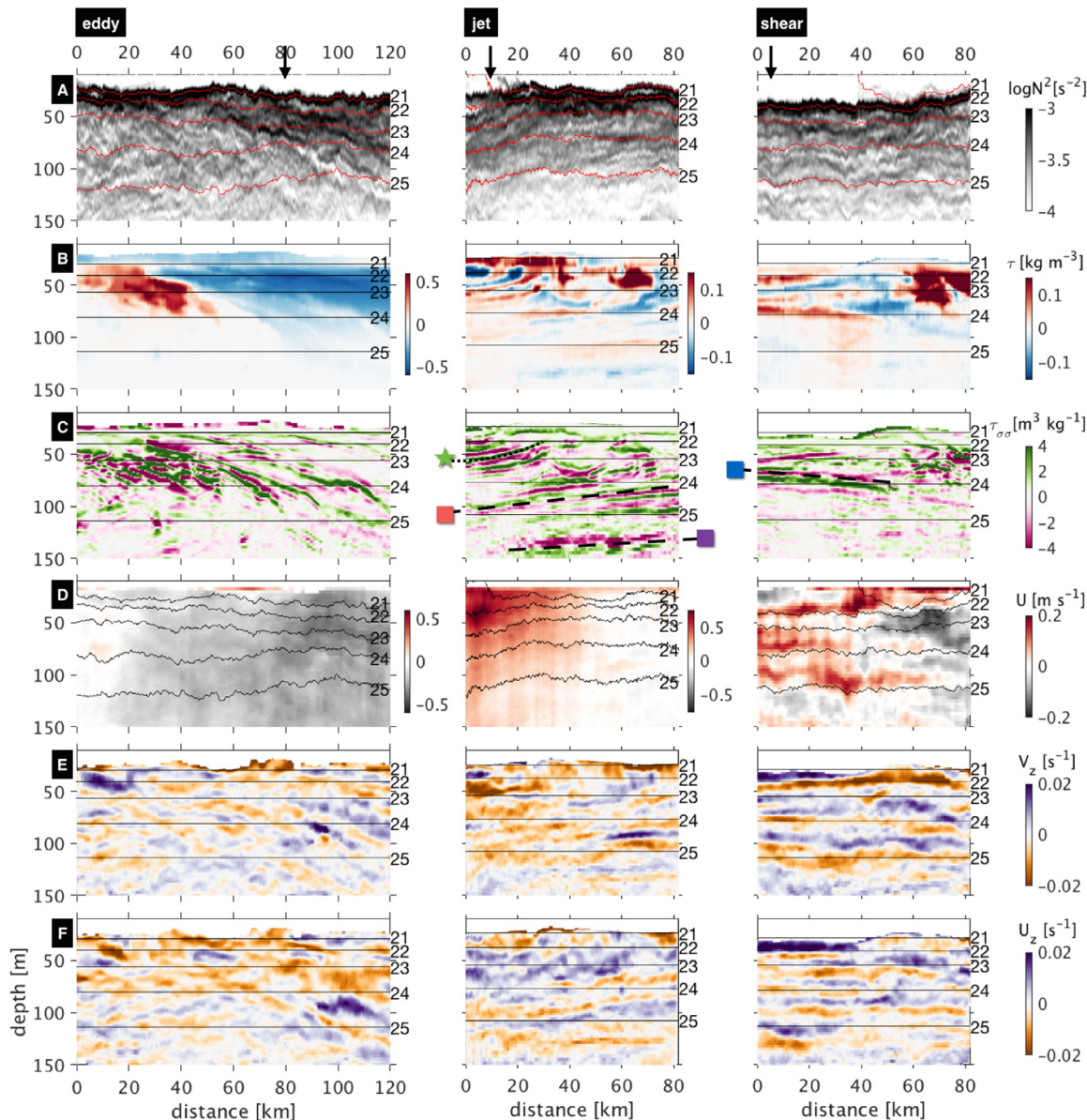


**Fig. 5.** Details from the sections shown in Fig. 2. ‘Eddy’, the southern edge of the negative SLA and the cyclonically rotating currents. ‘Jet’, crossing a strong (max  $\sim 1 \text{ m s}^{-1}$ ) and narrow jet of surface current. ‘Shear’, area with weak currents but prominent vertical shear layers. (A)  $\log_{10}$  of density stratification  $N^2$ . Red lines mark isopycnals 21 to 25  $\sigma$ . Black arrows mark the location of the  $T\bar{S}$  profiles shown in Fig. 7. (B) Isopycnal Spice  $\tau$ , plotted vs. the section average isopycnal depth, hence isopycnals (black lines) are flat. (C) Diapycnal Spiciness Curvature  $\tau_{ss}$ . The slanted dashed lines mark prominent layering, characteristics of which are shown in Fig. 8. (D) Across-track current velocity (red = out of the page) plotted vs. depth. (E) Vertical shear, across-track component and (F) along-track component, interpolated onto density and plotted vs. section-average isopycnal depth. (For interpretation of the references to colour in this figure legend, the reader is referred to the web version of this article.)

The sections through the eddy reveal an anomalously cold and fresh (‘minty’) watermass in the upper 100 m inside of the eddy (Fig. 2C). The minty interior has reduced DSC magnitudes and variance in contrast to the surrounding region (Fig. 2D). This indicates that the anomalous and uniform watermass in the eddy’s core coherently propagated with the eddy currents into the interior of the BoB. Satellite SLA maps before and after the cruise period reveal the cyclonic eddy had formed as a distinct isolated anomaly around 1st April 2015, near the northeastern corner of the BoB, traveled southwestward, and persisted as a distinct anomaly until merging into a coastal SLA feature around 1st February 2016, completing a 10-month-long journey (path marked in Fig. 1). When the ship crossed the cyclonic eddy, in September 2015 near  $88^\circ\text{E}$ , the eddy had already traveled roughly 5 months and 500 km from the northeastern edge of the BoB.

Spice reveals anomalous thermohaline structure below the surface mixed layer (Fig. 2C). For example, it highlights the fresh and cold

(minty) watermass lens in the core of the cyclonic eddy, between 1021 and 1024  $\text{kg/m}^3$  isopycnals, otherwise obscured by the large vertical gradient in  $S$  and  $T$ . South of the eddy, two salty and warm (spicy) patches stand out. Closer inspection of the spice patterns reveals smaller-scale horizontal variance, as seen north of the cyclonic minty eddy, or towards the southwestern end of the survey, where spice is vertically layered.

In contrast to the lack of watermass layering in the upper 100 m inside the eddy, DSC variance is elevated in several areas at the eddy’s periphery and outside of it. Three prominent layering features identified in Fig. 2, are associated with three prominent features in surface and subsurface currents. These are described as (i) ‘eddy’, at the periphery of the aforementioned mesoscale eddy, in between its cold-fresh interior watermass and a warm-salty watermass patch to the southwest of it; (ii) ‘jet’, the strong narrow current at the beginning of the cruise; (iii) ‘shear’, the final (southwestern) segment of the long

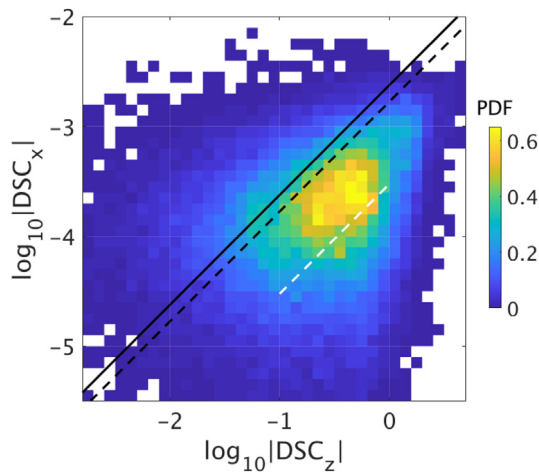


**Fig. 6.** Slopes of passive watermass tracer layers in the sections shown in Fig. 5, estimated by a 2D PDF of the vertical and horizontal gradients of DSC. For a given vertical gradient, a smaller horizontal gradient signifies a shallower slope. The black solid line corresponds to a slope of the average aspect ratio  $f/N \sim 2 \times 10^{-3}$  (dashed line  $f/\sqrt{2N}$ ) calculated between 50 m and 150 m depth, with  $N^2 = 10^{-3.5} \text{ s}^{-2}$ , and  $f(15^\circ) \sim 4 \times 10^{-5} \text{ s}^{-1}$ . The white dashed line indicates the average slope ( $3 \times 10^{-4}$ ) of the prominent layering marked by lines in Fig. 5.

section, which is marked by prominent shear layers (Fig. 2B). These segments are shown in detail in Fig. 5.

### 3.2. Slopes of layered watermass anomalies

In many cases, the features in watermass anomaly cross isopycnals. The three  $\sim 100$  km-long sections contain several different types of spice patterns (Fig. 5). For example, the ‘**eddy**’ segment, dominated by an along-isopycnal watermass gradient, shows many fragmented DSC anomalies that are sloping across isopycnals and are laterally coherent over scales  $\sim 30$  km. In contrast, the ‘**jet**’ segment contains DSC anomalies that are coherent over its entire 80 km length, also crossing isopycnals, but with a shallower slope. Similarly, the ‘**shear**’ segment contains nearly flat DSC layers that are coherent over at least 50 km, and possibly longer if they extend beyond the section that was observed. The distribution of slopes of the features with anomalous watermass signatures is shown in Fig. 6 by plotting the joint probability distribution of vertical and horizontal gradients of DSC. The center of the observed distribution corresponds to a slope of  $\sim 5 \times 10^{-4}$ , with a majority of the slopes smaller than  $1 \times 10^{-3}$ . The average slope of the prominent layers in the ‘**jet**’ section (marked by dashed lines in the third row of Fig. 5) is  $\sim 3 \times 10^{-4}$  and is marked by a white dashed line in Fig. 6.

### 3.3. Coincident stratification layering

In the three featured segments, layers of spice or watermass anomalies are accompanied by parallel sloping layers of anomalous density stratification. The coincidence of anomalies in spice and  $N^2$  can be seen in Fig. 7, which plots profiles from the region indicated by a black arrow (top row; Fig. 5) for each of the three segments termed ‘**eddy**’, ‘**jet**’, and ‘**shear**’. In Fig. 7, the upper 100 m of several adjacent vertical profiles are plotted in  $TS$  space. The profiles are colored by density stratification  $N^2$ , and its anomalies coincide with the wiggles in  $TS$  space, which correspond to spice anomalies. These wiggles do not necessitate any change in density, since changes in  $T$  can be fully density-compensated by changes in  $S$ . Similarly, changes in vertical density stratification can occur without any changes in spice, since a water column with a single  $TS$  profile can be vertically squeezed or stretched, changing only the vertical density gradient. However, in

these three sections, both spice and  $N^2$  show the same  $\sim 10$  m-spaced alternating anomalies with depth, with values of  $N^2$  alternating between a minimum of  $10^{-2} \text{ s}^{-2}$  and a maximum up to  $10^{-3} \text{ s}^{-2}$ . Yet the phase relationship between the anomalies is different for each of the three sections. For example, in the top 70 m of the ‘**jet**’ profiles, increased stratification anomalies coincide with the watermass switching from minty to spicy with increasing depth, whereas in the ‘**shear**’ profiles, the increased stratification anomaly coincides with minty anomalies.

### 3.4. Multiple parallel layers

Four instances of multiple parallel spice layers, coherent over tens of kilometers, stand out in the sections of Fig. 5. Marked by dashed lines in the ‘**jet**’ and ‘**shear**’ segments, properties of these layers are shown in Fig. 8. The prominent layering patterns are distinguished by the following characteristics: (i) shallow  $O(10^{-4})$  cross-isopycnal slopes, (ii) multiple, parallel,  $O(10)$ m-thin, layers in spice anomaly, (iii) lateral coherence that extends over scales of (at least, and probably exceeding) 30–80 km, and (iv) coincidence in layers of anomalies in  $N^2$  (density stratification) and spice (watermass).

### 3.5. Mechanisms for layer formation

#### 3.5.1. Mesoscale stirring

The large-scale distribution of spice layering in our observations, marked by suppressed DSC variance within the mesoscale eddy’s interior and elevated variance at the eddy’s edges, fits into the framework of mesoscale stirring of spice (Meunier et al., 2015). The lack of DSC variance in the eddy’s interior is consistent with trapped waters being advected coherently in the eddy core, the region of minimum mesoscale strain and shear. Consequently little to no spice layering has formed in the 5 months between the eddy’s origin in the BoB’s northeastern coastal region and our observations. In contrast, spice gradients at the eddy’s edges are multi-layered, consistent with strain and shear acting at the eddy’s edge. The salinity maximum at the eddy’s southern edge is likely a long salty filament advected by the mesoscale flow from the south (Fig. 1) that is stretched around by the eddy’s rotating currents and seen in cross-section.

The aspect ratio  $f/N$  in the stratified interior of the BoB (between 50 m and 150 m depth) was on average  $2 \times 10^{-3}$  (given  $f(15^\circ) \sim 4 \times 10^{-5} \text{ s}^{-1}$ , and average  $N = 0.02 \text{ s}^{-1}$ ). Alternatively, using the average mesoscale strain, which is of order  $10^{-5} \text{ s}^{-1}$  (calculated from AVISO currents), and the average observed shear magnitude of  $10^{-2} \text{ s}^{-1}$ , the strain to shear ratio is also estimated to be of  $O(10^{-3})$ . However, almost all observed tracer slopes are shallower than  $f/N$ , the theoretical slope expected from mesoscale stirring (black line in Fig. 6). The mean of the observed slopes ( $\sim 5 \times 10^{-4}$ ) is four-fold smaller than  $f/N$ . The most prominent layer slopes ( $\sim 3 \times 10^{-4}$ ) are an order of magnitude smaller than  $f/N$ . This finding is similar to observations made by Klymak et al. (2015), who hypothesized that the shallower aspect ratios indicated sources of stirring at depth, other than surface frontogenesis or low-mode quasi-geostrophic processes.

In what follows, we propose two alternate mechanisms to generate spice layering that could explain the observed layering patterns in anomalies of spice and  $N^2$  in the Bay of Bengal.

#### 3.5.2. Mechanism A: Submesoscale sheared eddy twist

The first proposed mechanism, which produces multiple parallel spice layers with a lateral extent of a few 10’s of km, involves stirring by a submesoscale eddy across a front of both spice and density. While stirring by any sheared flow, such as mesoscale currents with shear, can produce thin, sloping, spice layers, such currents cannot produce multiple parallel layers, unless initially there were multiple parallel vertical gradients (Franks, 1995). In contrast, a submesoscale eddy, formed at a front, can twist a single horizontal spice gradient around

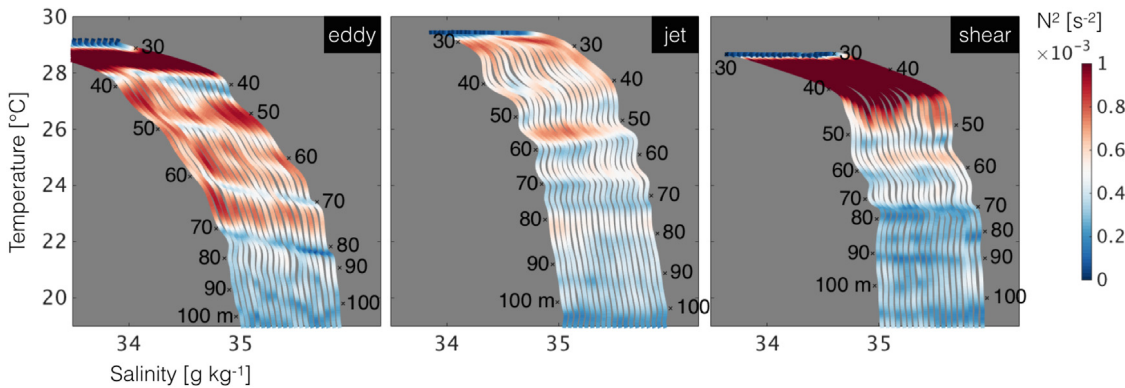


**Fig. 7.** *TS* profiles from the sections shown in Fig. 5, in the vicinity of the locations marked by black arrows. Each panel shows 19 consecutive profiles, spanning about 1 h and 6 km along the ship track, from the ‘*eddy*’, ‘*jet*’ and ‘*shear*’ sections. Color shading is indicative of density stratification  $N^2$ , while wiggles in the profiles are indicative of watermass anomalies. Anomalies in watermass and  $N^2$  have similar vertical and lateral coherence. Labels indicate the depth along the first and last profiles. Each consecutive profile is shifted slightly to the right (starting from the first profile) to generate this waterfall plot.

multiple times, creating multiple parallel layers on a time scale of days to weeks.

The region of the ‘*jet*’ section, traversed three times within about 36 h along a line perpendicular to the mesoscale flow (Fig. 9A), exhibited variability consistent with a submesoscale flow field. Surface-intensified, and with maximum observed speeds of  $1 \text{ m s}^{-1}$ , the observed jet was not restricted to the ML, and extended into the stratified pycnocline of the upper 50 m. Both the position, strength, and depth of the jet changed between each successive crossing. Estimates of vorticity, approximated by the along-track horizontal gradient of across-track currents, show elevated values greater than the planetary vorticity  $f$  in the first and third transects (Fig. 9B), in a narrow, 10 km wide section. The rapid timescale of flow evolution and the strong vorticity, indicate that the narrow jet is submesoscale in its dynamical character (Capet et al., 2008).

A vertically sheared, recirculating submesoscale eddy at a spice front would quickly produce layering. Illustrated by a kinematic model in Fig. 3A, the rotating, vertically sheared current (decaying in magnitude with increasing depth), simply tilts and twists the pre-existing spice front by multiple rotations, producing a new watermass layer with each turn.

Our numerical simulation with the Process Study Ocean Model (PSOM) starts with a front in density and spice, and a thermally balanced current or jet at the front, which becomes unstable and forms submesoscale eddies. This model demonstrates the formation of spice layering in the observed ‘*jet*’ section with a strong current. In the numerical simulation, the submesoscale frontal instability, with relative vorticity as large as the planetary vorticity  $f$ , grows to form an eddy within a few inertial periods (Fig. 3B). The eddy drags water parcels across the front, wrapping the spice into layers with each subsequent twist of the eddy as the flow evolves. A horizontal slice from the model of spice and vorticity in the stratified interior at 77 m depth (Fig. 10) shows the eddy with a strong positive vorticity anomaly stirring spice around. It also shows density stratification ( $N^2$ ) enhanced on one side of the eddy and diminished on the other side, coincident with the steepening and slumping of isopycnals as the eddy advects water across the front during the process of eddy-driven restratification of the front (Mahadevan et al., 2012).

The vertical shear (of the horizontal velocity) beneath the surface-intensified current (Fig. 3C) produces several layers of alternating spice below the front that are prominently visible in DSC (Fig. 3E). Furthermore, while the motion that produces the spice layering can be purely along-isopycnal and geostrophic, the eddy’s horizontal and vertical shear (Fig. 3F) in the simulation produces critical Richardson numbers (Fig. 3H) and  $O(1)$  Rossby numbers (Fig. 3G), thus ageostrophic components are likely not negligible. The eddy’s non-geostrophic currents can slump isopycnals. At the location where the submesoscale eddy currents

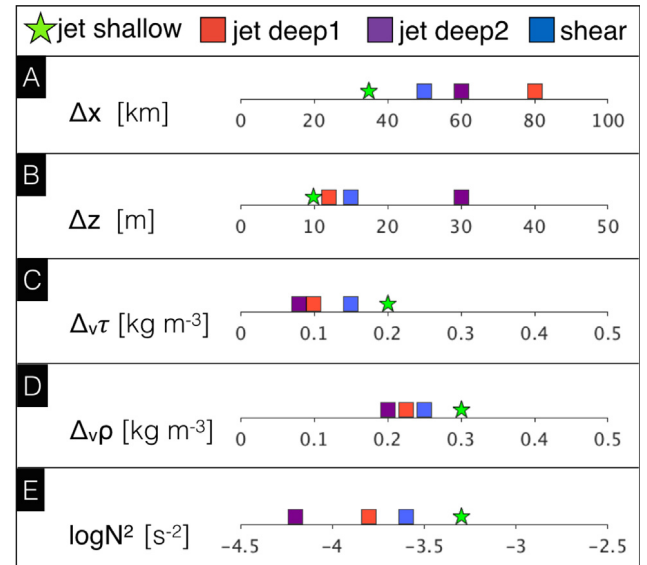


**Fig. 8.** Properties of the prominent layering marked in Fig. 5 by black dashed lines and corresponding symbols in the ‘*jet*’ and ‘*shear*’ sections; values are estimates with about 10% uncertainty. (A) Horizontal extent, lower limit, since the layering patterns likely extended beyond the end of the ship tracks. (B) Vertical thickness of individual layers within the patterns of multiple parallel layers. (C) Magnitude of the vertical spice anomaly. (D) Vertical change in density across thickness of individual layers. (E) Mean density stratification  $N^2$  at the depth of the layers.

push water from the lighter to the denser side of the front, isopycnals are slumped, and stratification is enhanced (Mahadevan et al., 2012). This process leads to layers of anomalous density stratification coincident with spice layering (Fig. 3B).

The hypothesized mechanism of submesoscale eddy twisting could form the shallow layering observed in the ‘*jet*’ area, as demonstrated by the process study model simulation. However, another mechanism for layer formation is more consistent with what is observed in the ‘*shear*’ section

### 3.5.3. Mechanism B: Near-inertial wave (NIW) shear

The ‘*shear*’ section in the transect, unlike the ‘*jet*’ section, does not contain fast currents, but is distinguished by prominent vertical shear layers that are around 10 m thin, nearly flat, and extend over 80 km length. The layers are seen as changes in shear direction (Fig. 2B), or as alternating anomalies in  $U_z$  and  $V_z$  (vertical gradient of across- and along-track current) in Fig. 5, extending from below the surface mixed

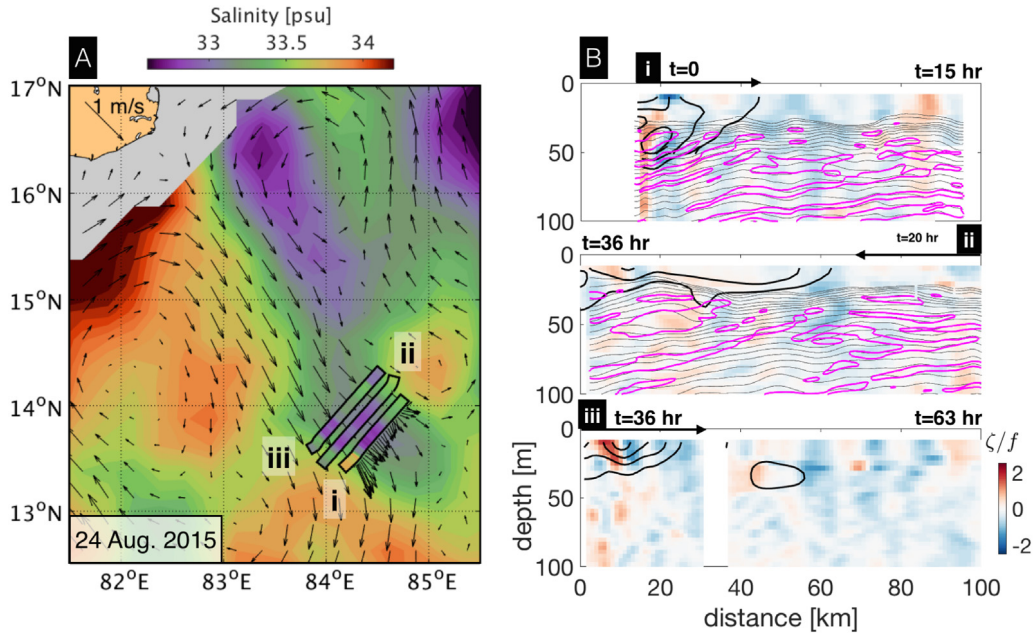


**Fig. 9.** Repeat transects across the fast jet shown in the inset of Fig. 1. (A) Surface geostrophic currents (arrows) and surface salinity (color) measured by satellite (background, SMAP salinity data from [www.remss.com](http://www.remss.com), Aviso + geostrophic current data from [www.aviso.altimetry.fr](http://www.aviso.altimetry.fr)) and the ship (transects i, ii, and iii, the latter two have been shifted NW in the plot) between August 24 and 27, 2015. Note that the surface density front (dominated by the salinity gradient) is oriented opposite to the implied density gradient at depth that is balanced by the mesoscale flow. (B) Background color shows the vertical vorticity component estimated as  $U_y$  (along-track gradient of across-track velocity) normalized by planetary vorticity  $f$ . Thick black lines contour current speeds above 50 cm s<sup>-1</sup> in 10 cm s<sup>-1</sup> increments. Thin lines mark isopycnals in 0.2  $\sigma$  increments. Magenta lines contour the layers of negative Diapycnal Spiciness Curvature (DSC)  $\tau_{\text{ss}}$ . Note the significant changes in jet locations and strengths between each of the 3 transects taken within 1.5 days of each other, which is less than one inertial period. FCTD TS profiling was conducted only during the first two transects.

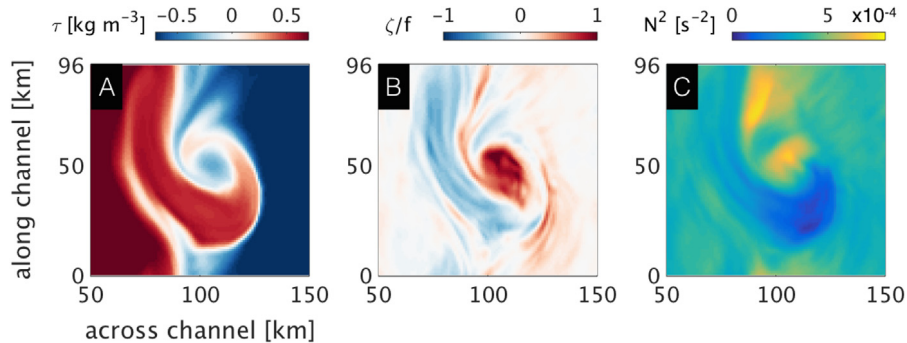


**Fig. 10.** Horizontal (x-y) slice at 77 m depth from the model shown in Fig. 3B, showing a submesoscale eddy stirring spice across a front. (A) Spice (B) Vorticity normalized by  $f$  (C) Stratification  $N^2$ .

layer to at least 150 m depth. In the upper 100 m, they are coincident and parallel with the observed layers of spice. To examine the relation between shear and spice anomalies, Fig. 4B shows a hodograph of an average shear profile (horizontally averaged over 10 km) of the two components  $U_z$  and  $V_z$ , colored by spice. The shear is neither rotating clearly clockwise nor counter-clockwise, but dominated by oscillations along one diagonal axis. The spice anomaly oscillates from positive at one end of the diagonal axis, to negative at the other, coherent with the shear anomalies.

Illustrated by a kinematic model in Fig. 4A, the vertically sheared flow, oscillating at each depth level in a clockwise progression of flow direction, simply interleaves the two watermasses at the spice front in layers of the same thickness as the vertical wavelength. Whether a section through this area reveals interleaving or parallel layering depends on the orientation of the section relative to the orientation of the spice front; a section along the front reveals multiple parallel layers in spice, a section across the front reveals interleaving of spice.

The magnitude of the alternating spice anomaly in the vertical depends on the sharpness of the pre-existing horizontal spice front, and

the horizontal displacement by the NIW. In the ‘shear’ section detail (Fig. 5), the vertical spice anomalies are of the same magnitude as the horizontal change in spice seen in the same section across a ~10 km gradient, both covering a spice range of about 0.2 kg m<sup>-3</sup>. We estimate the relative horizontal excursion between alternating shear layers by multiplying one half the inertial period (i.e.  $0.5 \times \sim 2$  days) by the relative speed between adjacent layers (estimated to be  $O(0.1)$  m s<sup>-1</sup> from the shear magnitude multiplied by vertical wavelength), which gives  $O(10)$  km horizontal displacements. The NIW interleaving can thus produce vertical spice anomalies of the observed magnitude.

While the oscillatory flow is mostly horizontal, the wave’s vertical component will nonetheless induce alternating anomalies of vertical strain (Alford et al., 2016). The vertical displacement needed to produce the observed magnitude of stratification anomalies is estimated by decomposing the vertical gradient of density (approximated to be smoothly increasing with depth) into a background and a wave strain component, such that  $N^2 = (-g/\rho_o) \frac{\partial \rho(z)}{\partial z} [1 + \frac{\partial}{\partial z} \xi]$ , where  $\xi$  is the vertical displacement due to the NIW, and its vertical derivative is strain. Relative stratification anomalies of 20%, observed for example in the

BoB sections, are produced by alternating vertical displacements of 2 m over 10 m vertical wavelengths, or strain  $\xi_z = 0.2$ . Such strain values are consistent with linear internal wave scaling of strain as  $\sim \omega^{-1}(k_x U + k_y V)$ , (Sun and Kunze, 1999) applied to near-inertial frequencies  $\omega$  of  $O(10^{-5})$  s $^{-1}$ , horizontal wavenumber ( $k_x, k_y$ ) corresponding to wavelengths of  $O(100)$  km, and relative horizontal velocities of  $O(0.1)$  m s $^{-1}$  in the ‘shear’ section (Fig. 5).

## 4. Discussion

### 4.1. Layering mechanisms in the Bay of Bengal

What is the source of the observed prominent, parallel, tens of kilometer long, very gently sloping layers of watermass and density stratification anomalies in the Bay of Bengal? High-wavenumber layering in instantaneous density stratification  $N^2$ , i.e. alternating anomalies of enhanced and diminished vertical gradients of density, is usually interpreted as the effect of vertical stretching and squeezing by internal gravity waves (IGW) (Garrett and Munk, 1979). But, such vertical displacements associated with IGWs do not create spice layering. On the other hand, mesoscale isopycnal stirring can generate spice layers, but does not create density stratification anomalies. In the Bay of Bengal, we observed coincident layering in both, as well as coincident shear layers of a similar vertical scale.

Double diffusive fluxes are thought to be able to create cross-isopycnal layering of spice as well as stratification anomalies (Rudnick and Turner, 1979). However, any double diffusive instability mechanism needs a vertical inversion of either salinity or temperature, or a compensated thermohaline front from which to extract energy (Schmitt, 1994). Here, across the upper 200 m, both salinity and temperature are generally stably stratified. The layering in the ‘jet’ and ‘shear’ sections is neither within a large-scale  $T$  or  $S$  inversion nor a thermohaline front, and thus unlikely to be created by salt fingering or diffusive convection instabilities. This does not rule out the possibility that double diffusion acts between the anomalous spice layers, because salinity profiles occasionally contain inversions caused by the layering. Double diffusive fluxes would reduce the magnitude of the spice anomalies, while producing alternating anomalies of weakened and strengthened density stratification. However, it is questionable if double-diffusive instabilities would grow in the highly sheared environment and we think it is unlikely to be the leading cause of the observed layers.

The two mechanisms that we propose, NIW shear and submesoscale sheared eddy twist, produce thin long layers of spice and  $N^2$  anomalies on a shorter timescale than mesoscale stirring. Their predicted horizontal extent, vertical thickness, formation time, and spice anomaly magnitude, summarized in Table 1, make them plausible mechanisms for the observed layering.

The properties of layers formed by submesoscale sheared eddy twist are time dependent. Every full rotation of an eddy increases the number of layers by one, between the surface and the depth ( $H$ ) at which the eddy current is negligible. The formation timescale of  $n$  layers is dependent on the eddy rotation rate, estimated by the width of the eddy ( $L$ ) divided by the maximum current magnitude ( $U_{max}$ ). The resultant scale,  $\sim nL/U_{max}$ , can also be expressed as a function of vorticity as  $\sim n/\zeta$ , by approximating the vorticity magnitude as  $U_{max}/L$ .

Based on the observed characteristics of the shallow layering in the ‘jet’ section (Fig. 9), with  $\sim 5$  spice layers beneath a jet with  $O(f)$  vorticity, and accounting for a factor of  $2\pi$ , the timescale of formation is estimated as  $5 \cdot 2\pi/4 \times 10^{-5}$  s, or roughly 10 days ( $\sim 2$  days per eddy rotation). While the lateral scale of layers depends on the size of the eddy  $L$ , the vertical thickness of these layers is proportional to the depth of the eddy  $H$  (depth over which the surface intensified currents decay), divided by the number of layers  $n$ . In the jet observations, with the strong current restricted to the top  $\sim 75$  m (Fig. 9), a 10 m vertical

thickness for  $\sim 5$  layers is in line with our scaling estimate of  $\sim 75/5$ , or about 15 m.

In contrast, a mesoscale eddy with weaker vorticity would take 10 times longer to form multiple vertical layers by twisting an existing horizontal spice gradient. For example, an eddy 200 km across with current magnitudes of 0.5 m s $^{-1}$  decaying linearly over the top 100 m, would need  $\sim 100$  days to create 4 layers of 25 m vertical thickness each. Submesoscale eddies with  $O(1)$  Rossby numbers create layering 10 times faster than mesoscale eddies.

Layers created by the sheared eddy twist mechanism have a thickness  $H/n$  that decreases with time, inversely proportional to the formation timescale. In the above example, the submesoscale jet created  $\sim 10$  m thick layers in about 10 days, and would create  $\sim 5$  m thick layers in 30 days, or  $\sim 1$  m thick in 2–3 months. The thinness might be limited by the scale of isotropic turbulent mixing events, such as breaking internal waves, independent of a (low) time-mean value of diffusivity observed in the BoB.

Unlike the time-dependent properties of layers created by the sheared eddy twist mechanism, the properties of NIW shear induced layers are closely and simply related to the wave characteristics. Layers with vertical thickness equal to the vertical shear wavelength, and lateral extent equal to the NIW lateral extent (or, if shorter, the spice front length), form on the timescale of the local inertial period  $\sim 2\pi/f$ , or about 2 days in the BoB. The interleaving is expected to be reversed a half-period later, however with the superposition of other currents and shears, the watermass layering does not necessarily fully reverse.

Thus, a low-frequency, high-vertical wavenumber wave can produce multiple parallel layers of spice and stratification anomalies. We propose this mechanism as a possible source of the observed layering in the ‘shear’ section, as well as of the similar layering observed below 75 m in the ‘jet’ section.

The source of the observed NIW could be either downward propagating energy from atmospheric wind forcing, or energy radiating from the frontal jet, for example by a loss of balance of the flow (Alford et al., 2013). The atmospheric forcing during the August–September 2015 cruise, in the late summer monsoon season, contained impulsive and strong wind changes that stimulated NIWs, see Adams et al. (2019). The forcing was marked by both weak ( $< 5$  m s $^{-1}$ ) and strong ( $> 10$  m s $^{-1}$ ) wind speeds with variable direction. A rotary spectral decomposition of vertical shear profiles (Rainville and Pinkel, 2004) collected during the cruise, shows that on average, clockwise oscillations dominate, with vertical scales of  $O(10)$  m (Fig. 4), indicative of downward propagating surface-forced NIWs. Furthermore, NIWs were separately observed in the BoB by Johnston et al. (2016) and just prior to the beginning of the observations analyzed in this manuscript (Adams et al., 2019).

To identify and distinguish these two potential layering mechanisms in action, hydrographic observations are needed that track layers over time, ideally for at least a full inertial period. Subsurface waters exhibiting layering patterns could be sampled with short sections of vertical profiles of  $T$ ,  $S$ , and shear, and followed as the layers are potentially advected by mesoscale flows and tides. Such observations would verify whether the spice layers reverse and evolve with a coincident near-inertial oscillation, whether they increase in wavenumber as a surface eddy adds twists of alternating watermass from above, or whether they are independent of both NIW and eddy rotations, evolving only slowly as a passive feature sheared by the mesoscale flow.

### 4.2. Implications for mixing in the Bay of Bengal

The prominent spice layering observed in the BoB, characterized by multiple thin parallel layers in DSC, stratification, and shear, suggests that submesoscale and NIW phenomena are prevalent, and play a central role in stirring the upper ocean. The observed spice and shear layering, with only 10 m vertical wavelengths (but at least 80 km horizontal extent in one instance), draws attention to NIWs with a much higher wavenumber than the majority of NIWs studied (Alford et al.,

**Table 1**

Table summarizing the predicted properties of spice layering produced by the proposed mechanisms: interleaving by NIWs (Fig. 4A), and layering by a submesoscale sheared eddy twist (Fig. 3A).

#### Interleaving layers in the Bay of Bengal

Layering	Near inertial wave shear	Submesoscale sheared eddy twist
Lengthscale $\Delta x$	horizontal wavelength, or length of spice front	Diameter of eddy $\sim L$
Timescale	Inertial period $\sim 1/f$	1 layer per rotation: $N \text{ layers} \cdot \text{Period}_{\text{rotation}} \approx (N \cdot L/U_{\max})$
Thickness $\Delta z$	Vertical wavelength	Eddy depth $H \cdot 1/N_{\text{layers}}$ $\approx H \cdot L/(U \cdot t_{\text{elapsed}})$
Spice anom. $\Delta_v \tau$	$\sim \nabla_{\text{hor}} \tau \cdot  \text{Shear}  \cdot 1/f$	$\sim \nabla_{\text{hor}} \tau \cdot L$

2016), although they are consistent with independent but concurrent observations in the region (e.g. Adams et al. (2019), Lucas et al. (2016)). Near-inertial oscillations were proposed (Beal, 2007) as a source of interleaving in the Agulhas front, but for spice layers an order of magnitude thicker. Yet higher-wavenumber waves might be especially effective at contributing to shear dispersion, since the thinner layers can be vertically homogenized by turbulent mixing more rapidly than thicker layers. During the cruise of August–September 2015, vertical shear was observed to contain significant downward-propagating modes with  $O(10)$  m vertical wavelengths. Perhaps, a larger than usual portion of energy input by winds into NIWs in the BoB is contained in high-vertical-wavenumber modes, increasing the effectiveness of shear dispersion on horizontal mixing (Young et al., 1982).

The large aspect ratio or nearly-flat slopes of the prominent layers, of  $O(10)$  m thickness and  $O(10)$  km lateral scales, implies that diapycnal mixing, however weak, is effectively “mixing” at much larger horizontal scales when it vertically mixes such gently sloping features (Sundermeyer and Ledwell, 2001). If the source mechanism of these layers were mesoscale lateral strain and vertical shear (Haynes and Anglade, 1997), or small-scale strain and shear (Smith and Ferrari, 2009), the thinness of the layers would indicate very weak turbulent mixing that permits tracer features to cascade to high vertical wavenumbers before being mixed. Indeed observations of turbulence in the BoB reveal very weak average mixing levels (Shroyer et al., 2016; Lucas et al., 2016).

The formation timescale of layering produced by the submesoscale eddy-twist or the NIW-shear mechanisms is of the order of a few inertial periods. The flatter slopes of  $O(10^{-4})$  imply a tenfold increase in the horizontal scale at which turbulent mixing effectively reduces horizontal gradients by shear dispersion, compared to regimes where only mesoscale stirring creates sloping tracer features with average slopes of  $O(f/N)$ . If these submesoscale eddies or NIW processes also incidentally enhance vertical mixing by increasing fine-scale shear (Garrett and Munk, 1972), then the formation of these thin layers represents a potential source of horizontal stirring that leads to mixing at sub-mesoscales, in addition to dispersion driven by mesoscale currents in the BoB. Submesoscale and NIW dynamics are potentially the rate-controlling processes for the formation of vertical gradients.

Of further interest in the ‘jet’ section is the presence of deep spice layering, perhaps created by NIW shear, given its similarity to the ‘shear’ section described above. This raises two additional possible interpretations of the layering in this region. The implied NIW could have been directly forced by energy radiating from the front (Alford et al., 2013; Nagai et al., 2015). We indeed observe time-dependence of the narrow and fast current, potentially transferring energy from balanced motions to waves. Additionally, the shallow layering below the front could also have been caused by a NIW, but altered and steepened by interactions between the oscillations of the wave and the baroclinic submesoscale flow (Whitt and Thomas, 2013). The large vorticity values, both positive and negative, surrounding the jet could alter the propagation and characteristics of NIWs. Interesting questions remain about NIW modes with high vertical wavenumbers, specifically

regarding their generation and interactions. The role of the unusually strong and shallow density stratification in modulating surface near-inertial forcing, the potential source of NIWs by adjustments of frontal jets, and the interactions of NIWs with high-vorticity submesoscale fronts, are topics that would benefit from further modeling simulations and observational work in the BoB.

## 5. Concluding remarks

Observations from the upper 200 m of the Bay of Bengal over several 20–100 km long sections reveal thermohaline patterns of multiple, parallel,  $\sim 10$  m thin layers that cross isopycnals, and have slopes of  $O(10^{-4})$  that are shallower than  $f/N$ . Along with the watermass layering, which can be discerned from anomalies in spice or DSC, we observe coincident and parallel anomalies in density stratification and layering in the vertical shear orientation. The characteristics of these patterns lead us to propose two specific mechanisms previously not considered in the formation of thermohaline layering of this type. Submesoscale eddies formed at a density front with a vertically sheared flow can stir a spice gradient and twist the watermasses into layers. The process can generate corresponding anomalies in stratification due to the slumping of isopycnals or restratification of the front. Alternately, near-inertial waves with a high vertical wavenumber generate predominantly horizontal rotary oscillations that act on a spice gradient to cause layered interleaving that would theoretically reverse over an inertial period. The vertical strain field of the near-inertial wave acts to squeeze and stretch layers lying one above another, thereby generating coincident density stratification. A combination of these mechanisms could be contributing to the observed layering patterns.

The small vertical scales ( $\sim 10$  m), sharp vertical gradients in watermass properties, large lateral extents (tens of km), and the relatively short formation timescale of these watermass layers (days to weeks) implies that vertical diapycnal mixing can contribute to effective horizontal tracer mixing on larger scales than is feasible in the absence of these layering processes.

## Declaration of competing interest

The authors declare that they have no known competing financial interests or personal relationships that could have appeared to influence the work reported in this paper.

## CRediT authorship contribution statement

**Gualtiero Spiro Jaeger:** Conceptualization, Methodology, Visualization, Writing - original draft. **Andrew J. Lucas:** Investigation, Resources, Funding acquisition, Writing - review & editing. **Amala Mahadevan:** Software, Methodology, Funding acquisition, Writing - review & editing, Supervision.

## Acknowledgments

We are grateful to the captain and crew of the *R/V Roger Revelle* and for the international collaborative group ASIRI-OMM scientists, technical staff, and support personnel, but especially for those that sat long watches at the Fast-CTD console or on the rail. This work was supported by the U.S. Office of Naval Research under the following grants: N00014-16-1-2470, N00014-13-1-0451 (G.S.J. and A.M.) and N00014-13-1-0489, N00014-17-1-2391 (A.J.L.). The authors would like to specifically acknowledge the leadership of Dr. Terri Paluszewicz in realizing the complex multi-year project of which this effort is a small part. All authors declare that they have no competing interests.

## References

- Adams, K., MacKinnon, J., Lucas, A.J., Nash, J., Shroyer, E., Farrar, J.T., 2019. Multi-platform observations of small-scale lateral mixed layer variability in the northern Bay of Bengal. *Deep Sea Res. II* 104629. <http://dx.doi.org/10.1016/j.dsr2.2019.07.017>.
- Alford, M.H., MacKinnon, J.A., Simmons, H.L., Nash, J.D., 2016. Near-inertial internal gravity waves in the ocean. *Annu. Rev. Mar. Sci.* 8, 95–123.
- Alford, M.H., Shcherbina, A.Y., Gregg, M.C., 2013. Observations of near-inertial internal gravity waves radiating from a frontal jet. *J. Phys. Oceanogr.* 43 (6), 1225–1239.
- Beal, L.M., 2007. Is interleaving in the agulhas current driven by near-inertial velocity perturbations? *J. Phys. Oceanogr.* 37 (4), 932–945.
- Capet, X., McWilliams, J.C., Molemaker, M.J., Shchepetkin, A., 2008. Mesoscale to submesoscale transition in the California current system. Part II: Frontal processes. *J. Phys. Oceanogr.* 38 (1), 44–64.
- Charney, J.G., 1971. Geostrophic turbulence. *J. Atmos. Sci.* 28 (6), 1087–1095.
- Cole, S.T., Rudnick, D.L., 2012. The spatial distribution and annual cycle of upper ocean thermohaline structure. *J. Geophys. Res.: Oceans* 117 (C2).
- d'Orgeville, M., Hua, B.L., Schopp, R., Bunge, L., 2004. Extended deep equatorial layering as a possible imprint of inertial instability. *Geophys. Res. Lett.* 31 (22).
- Flament, P., 2002. A state variable for characterizing water masses and their diffusive stability: spiciness. *Prog. Oceanogr.* 54 (1–4), 493–501.
- Franks, P.J., 1995. Thin layers of phytoplankton: a model of formation by near-inertial wave shear. *Deep Sea Res. I* 42 (1), 75–91.
- Garrett, C., 1979. Mixing in the ocean interior. *Dyn. Atmos. Oceans* 3 (2–4), 239–265.
- Garrett, C., Munk, W., 1972. Oceanic mixing by breaking internal waves. In: *Deep Sea Research and Oceanographic Abstracts*, vol. 19, no. 12. Elsevier, pp. 823–832.
- Garrett, C., Munk, W., 1979. Internal waves in the ocean. *Annu. Rev. Fluid Mech.* 11 (1), 339–369.
- Haynes, P., Anglade, J., 1997. The vertical-scale cascade in atmospheric tracers due to large-scale differential advection. *J. Atmos. Sci.* 54 (9), 1121–1136.
- Jaeger, G.S., Mahadevan, A., 2018. Submesoscale-selective compensation of fronts in a salinity-stratified ocean. *Sci. Adv.* 4 (2), e1701504. <http://dx.doi.org/10.1126/sciadv.1701504>.
- Johnston, T.S., Chaudhuri, D., Mathur, M., Rudnick, D.L., Sengupta, D., Simmons, H.L., Tandon, A., Venkatesan, R., 2016. Decay mechanisms of near-inertial mixed layer oscillations in the Bay of Bengal. *Oceanography* 29 (2), 180–191.
- Klymak, J.M., Crawford, W., Alford, M.H., MacKinnon, J.A., Pinkel, R., 2015. Along-isopycnal variability of spice in the North Pacific. *J. Geophys. Res.: Oceans* 120 (3), 2287–2307.
- Lucas, A.J., Nash, J.D., Pinkel, R., et al., 2016. Adrift upon a salinity-stratified sea: A view of upper-ocean processes in the Bay of Bengal during the southwest monsoon. *Oceanography* 29.
- MacVean, M., Woods, J., 1980. Redistribution of scalars during upper ocean frontogenesis: A numerical model. *Q. J. R. Meteorol. Soc.* 106 (448), 293–311.
- Mahadevan, A., 2006. Modeling vertical motion at ocean fronts: Are nonhydrostatic effects relevant at submesoscales? *Ocean Model.* 14 (3–4), 222–240.
- Mahadevan, A., D'Asaro, E., Lee, C., Perry, M.J., 2012. Eddy-driven stratification initiates north atlantic spring phytoplankton blooms. *Science* 337 (6090), 54–58. <http://dx.doi.org/10.1126/science.1218740>.
- Mahadevan, A., Olinger, J., Street, R., 1996. A nonhydrostatic mesoscale ocean model. Part I: Well-posedness and scaling. *J. Phys. Oceanogr.* 26 (9), 1868–1880.
- Meunier, T., Ménesguen, C., Schopp, R., Le Gentil, S., 2015. Tracer stirring around a meddy: The formation of layering. *J. Phys. Oceanogr.* 45 (2), 407–423.
- Nagai, T., Tandon, A., Kunze, E., Mahadevan, A., 2015. Spontaneous generation of near-inertial waves by the Kuroshio front. *J. Phys. Oceanogr.* 45 (9), 2381–2406.
- Pinkel, R., Buijsman, M., Klymak, J.M., 2012. Breaking topographic lee waves in a tidal channel in Luzon Strait. *Oceanography* 25 (2), 160–165.
- Pinkel, R., Rainville, L., Slater, E., Goldin, A., Green, L., Bui, M., Aja, T., 2003. The hydrographic Doppler sonar system on the Roger Revelle. In: *Current Measurement Technology*, 2003. Proceedings of the IEEE/OES Seventh Working Conference on. IEEE, pp. 237–239.
- Rainville, L., Pinkel, R., 2004. Observations of energetic high-wavenumber internal waves in the kuroshio. *J. Phys. Oceanogr.* 34 (7), 1495–1505.
- Richards, K., Edwards, N., 2003. Lateral mixing in the equatorial Pacific: The importance of inertial instability. *Geophys. Res. Lett.* 30 (17).
- Ruddick, B., Turner, J., 1979. The vertical length scale of double-diffusive intrusions. *Deep Sea Res. A* 26 (8), 903–913.
- Schmitt, R.W., 1994. Double diffusion in oceanography. *Annu. Rev. Fluid Mech.* 26 (1), 255–285.
- Schmitt, R.W., Perkins, H., Boyd, J., Stalcup, M., 1987. C-SALT: an investigation of the thermohaline staircase in the western tropical North Atlantic. *Deep Sea Res. A* 34 (10), 1655–1665.
- Shcherbina, A.Y., Gregg, M.C., Alford, M.H., Harcourt, R.R., 2009. Characterizing thermohaline intrusions in the north pacific subtropical frontal zone. *J. Phys. Oceanogr.* 39 (11), 2735–2756.
- Shroyer, E.L., Gordon, A.L., Jaeger, G.S., Freilich, M., Waterhouse, A.F., Farrar, J.T., Sarma, V., Venkatesan, R., Weller, R.A., Moum, J.N., Mahadevan, A., 2019. Upper layer thermohaline structure of the Bay of Bengal during the 2013 northeast monsoon. *Deep Sea Res. II* <http://dx.doi.org/10.1016/j.dsr2.2019.07.018>.
- Shroyer, E.L., Rudnick, D.L., Farrar, J.T., Lim, B., Venayagamoorthy, S.K., St. Laurent, L.C., Garanaik, A., Moum, J.N., 2016. Modification of upper-ocean temperature structure by subsurface mixing in the presence of strong salinity stratification. *Oceanography* 29 (2), 62–71.
- Smith, K., Ferrari, R., 2009. The production and dissipation of compensated thermohaline variance by mesoscale stirring. *J. Phys. Oceanogr.* 39 (10), 2477–2501.
- Sun, H., Kunze, E., 1999. Internal wave-wave interactions. Part I: The role of internal wave vertical divergence. *J. Phys. Oceanogr.* 29 (11), 2886–2904.
- Sundermeyer, M.A., Ledwell, J.R., 2001. Lateral dispersion over the continental shelf: Analysis of dye release experiments. *J. Geophys. Res.: Oceans* 106 (C5), 9603–9621.
- Toole, J.M., McDougall, T.J., 2001. Chapter 5.2 Mixing and stirring in the ocean interior. In: *International Geophysics*, vol. 77. Elsevier, pp. 337–355.
- Whitt, D.B., Thomas, L.N., 2013. Near-inertial waves in strongly baroclinic currents. *J. Phys. Oceanogr.* 43 (4), 706–725.
- Young, W., Rhines, P., Garrett, C., 1982. Shear-flow dispersion, internal waves and horizontal mixing in the ocean. *J. Phys. Oceanogr.* 12 (6), 515–527.